Near-Infrared-to-Blue Upconversion in Colloidal $BaYF_5:Tm^{3+}$, Yb^{3+} Nanocrystals

Fiorenzo Vetrone, Venkataramanan Mahalingam, and John A. Capobianco*

Department of Chemistry and Biochemistry, Concordia University, Montreal, Quebec H4B 1R6, Canada

Received December 3, 2008. Revised Manuscript Received March 16, 2009

Tetragonal barium yttrium fluoride ($BaYF_5$) nanocrystals doped with 0.5 mol % Tm^{3+} and 15 mol % Yb^{3+} ($BaYF_5:Tm^{3+}$, Yb^{3+}) were synthesized using the thermal decomposition method yielding rectangular-shaped nanocrystals (15 nm × 5 nm) that can (up)convert near-infrared light to higher energies such as blue, via a process known as upconversion. The upconversion spectrum of the $BaYF_5:Tm^{3+}$, Yb^{3+} nanocrystals, following excitation with 980 nm, revealed that the upconverted blue emission from the $^1G_4 \rightarrow {}^3H_6$ transition was more intense than the infrared $^3H_4 \rightarrow {}^3H_6$ emission at high excitation densities (90 W/cm^2) contrary to what is normally observed for Tm^{3+}/Yb^{3+} codoped nanomaterials. On the other hand, the infrared emission dominates at lower excitation densities (15 W/cm^2) demonstrating a lack of excited Yb^{3+} ions to carry on the upconversion beyond the $^3H_4$ excited state to the $^1G_4$ excited state. A saturation of the upconversion process was observed in the power dependence studies at excitation densities above 57 W/cm^2, causing a deviation in the expected number of photons required for the upconversion process. The upconversion properties of $BaYF_5:Tm^{3+}$, Yb^{3+} nanocrystals are elucidated and discussed.

Introduction

There has been a surge of recent publications in the literature on luminescent lanthanide (Ln^{3+})-doped nanocrystals.[1−5] These luminescent nanocrystals are unique in that they can convert low-energy radiation (typically near-infrared) to higher energies such as visible or UV via a process known as upconversion.[6] This multiphoton process occurs because many of the tripositive lanthanide ions have a multitude of electronic energy states, which span the near-infrared (NIR) to the UV (and even beyond), many of which are equally spaced. In a typical multiphoton upconversion process, the Ln^{3+} ion embedded in a low-vibrational host is excited using NIR light (usually 980 nm) to an intermediate excited state, whereas a second NIR photon subsequently excites the ion to a even higher excited state. As a consequence of doping in a solid-state matrix, the lifetime of the first intermediate state of the Ln^{3+} ion is typically quite long (usually in milliseconds) and thus, acts as a population reservoir thereby facilitating the upconversion process. Unlike other two-photon absorption (TPA) materials, the intermediate states are real and thus, conversion of NIR light to higher energies can be accomplished simply with a small, low power, NIR diode eliminating the need for expensive and cumbersome ultrafast pulsed lasers.[7]

Typically in upconversion materials, the Yb^{3+} ion is added as a codopant to the matrix. The Yb^{3+} ion's single electronic excited-state is located at approximately 10 000 cm^{-1}, which is resonant with many inexpensive laser diodes, and has a higher extinction coefficient relative to the other Ln^{3+} ions.[8] Thus, when codoped with ions that have a resonant electronic energy state (i.e., Er^{3+}, Tm^{3+}, Ho^{3+}, Pr^{3+}), Yb^{3+} is an ideal sensitizer and enhances the efficiency of the upconversion process as it actively transfers the absorbed energy to the other codopants. Moreover, the Yb^{3+} ion can also cause upconversion to occur in cases where it is not normally observed in the single ion. The classic examples are Eu^{3+} and Tb^{3+}, which alone have no energy states capable of absorbing 980 nm; however, when codoped with Yb^{3+}, upconverted visible emission can be observed.[9,10]

When dispersed in solution, upconverting nanocrystals are suitable for a wealth of applications but above all in biology where the NIR excitation results in almost zero background. While preliminary studies demonstrate the extraordinary potential of these nanocrystals (typically $NaYF_4$)[11−16] there still exists a need to explore other colloidal Ln^{3+}-doped

* Corresponding author. E-mail: capo@vax2.concordia.ca.

(1) Boyer, J. C.; Vetrone, F.; Cuccia, L. A.; Capobianco, J. A. *J. Am. Chem. Soc.* **2006**, *128*, 7444–7445.
(2) Schäfer, H.; Ptacek, P.; Zerzouf, O.; Haase, M. *Adv. Funct. Mater.* **2008**, *18*, 2913–2918.
(3) Sivakumar, S.; van Veggel, F. C. J. M.; May, P. S. *J. Am. Chem. Soc.* **2007**, *129*, 620–625.
(4) Wang, X.; Zhuang, J.; Peng, Q.; Li, Y. *Nature (London)* **2005**, *437*, 121–124.
(5) Yi, G.; Chow, G. *Chem. Mater.* **2007**, *19*, 341–343.
(6) Scheps, R. *Prog. Quant. Electron.* **1996**, *20*, 271–358.
(7) König, K. *J. Microsc.* **2000**, *200*, 83–104.
(8) Wybourne, B. G., *Spectroscopic Properties of Rare Earths*; Wiley-Interscience: New York, 1965.
(9) Menezes, L. d. S.; Maciel, G. S.; de Araújo, C. B.; Messaddeq, Y. *J. Appl. Phys.* **2003**, *94*, 863–866.
(10) Sivakumar, S.; van Veggel, F. C. J. M.; Raudsepp, M. *J. Am. Chem. Soc.* **2005**, *127*, 12464–12465.
(11) Chatterjee, D.; Rufaihah, A.; Zhang, Y. *Biomaterials* **2008**, *29*, 937–943.
(12) Chen, Z.; Chen, H.; Hu, H.; Yu, M.; Li, F.; Zhang, Q.; Zhou, Z.; Yi, T.; Huang, C. *J. Am. Chem. Soc.* **2008**, *130*, 3023–3029.
(13) Lim, S. F.; Riehn, R.; Ryu, W. S.; Khanarian, N.; Tung, C.; Tank, D.; Austin, R. H. *Nano Lett.* **2006**, *6*, 169–174.
(14) Nyk, M.; Kumar, R.; Ohulchanskyy, T. Y.; Bergey, E. J.; Prasad, P. N. *Nano Lett.* **2008**, *8*, 3834–3838.
(15) Wang, F.; Liu, X. *J. Am. Chem. Soc.* **2008**, *130*, 5642–5643.
(16) Wang, L.; Yan, R.; Huo, Z.; Wang, L.; Zeng, J.; Bao, J.; Wang, X.; Peng, Q.; Li, Y. *Angew. Chem., Int. Ed.* **2005**, *44*, 6054–6057.

10.1021/cm900313s CCC: $40.75
Published on Web 04/14/2009

nanocrystals. It is known that the luminescent spectra of Ln^{3+}-doped nanocrystals (and Ln^{3+}-doped materials in general) vary little from host to host.[17] However, the crystal field exerted on the Ln^{3+} dopant ions by the host (nano)matrix plays a pivotal role in determining transition probabilities, lifetimes of the excited states, luminescence efficiency, as well as energy transfer efficiency.[18] Barium yttrium fluoride ($BaYF_5$) is a particularly promising host material for doping with Ln^{3+} ions and has not been studied in detail at the nanoscale. In the bulk, $BaYF_5$:Er^{3+}, Yb^{3+} is an excellent upconverting material and has been shown to be a factor of 8 more efficient than LaF_3:Er^{3+}, Yb^{3+}.[19,20] Furthermore, pioneering upconversion experiments on the $Yb^{3+}-Tm^{3+}$ couple doped in $BaYF_5$ have demonstrated blue emission with a cubic dependence on pump power and confirmed the hypothesis set forth of energy transfer between Yb^{3+} and Tm^{3+} ions with phonon assistance.[20,21] Furthermore, the blue upconverted emission was found to easily saturate at relatively low excitation powers. The phonon energy (vibrational energy) of the host matrix plays a key role in Tm^{3+}/Yb^{3+} upconversion as it must be large enough to assist in energy transfer as well as undergo multiphonon relaxation from excited states to lower lying states (such that alternate levels can undergo the upconversion process) yet be small enough to prevent multiphonon assisted quenching.[21] In this regard, $BaYF_5$ is an ideal host for the Tm^{3+}/Yb^{3+} codopants; however, the upconversion properties of the low-vibrational host $BaYF_5$:Tm^{3+}, Yb^{3+} at the nanoscale has yet to be reported.

Here, we report on the synthesis and luminescence properties of colloidal barium yttrium fluoride ($BaYF_5$) nanocrystals doped with Tm^{3+} and codoped with Yb^{3+}, which produces upconverted blue light following excitation with NIR light (980 nm).

Experimental Section

2.1. Synthesis of $BaYF_5$:Tm^{3+} 0.5 mol %, Yb^{3+} 15 mol % Nanocrystals. The $BaYF_5$:Tm^{3+} 0.5 mol %, Yb^{3+} 15 mol % nanocrystals were synthesized using the thermal decomposition method.[1,22] Briefly, the lanthanide (Y^{3+}, Tm^{3+}, Yb^{3+}) trifluoroacetates [prepared by reacting Y_2O_3 (0.92 mmol), Tm_2O_3 (0.0052 mmol), Yb_2O_3 (0.162 mmol), and 50% CF_3COOH v/v with water] were mixed with barium acetylacetonate (1.0 g); a coordinating solvent, oleic acid (20 mL); and a noncoordinating solvent, 1-octadecene (20 mL). The resulting mixture was heated to 110 °C with constant stirring under a vacuum. After 20 min, the temperature of the mixture was increased to 300 °C at the rate of 5 °C/min under an argon flow. At this final temperature, the mixture was allowed to stay for 1 h. Following this heat treatment, the colloidal mixture was cooled to 70 °C and was proceeded by the addition of absolute ethanol to precipitate the nanocrystals. The obtained nanocrystals were separated by centrifugation and further purified by dispersing them with hexane followed by precipitation with ethanol. A 2 wt % colloidal dispersion in toluene was prepared for the spectroscopic measurements.

2.2. Upconversion Luminescence Spectroscopy. Upconverted visible emissions were obtained upon excitation with 980 nm using a Coherent 6-pin fiber-coupled F6 series 980 nm laser diode (maximum power of 800 mW at 1260 mA), coupled to a 100 μm (core) fiber. For the spectroscopic studies, the sample was dispersed in toluene and placed in a Hellma, QS quartz cuvette (1 cm path length). The upconverted visible emissions were collected at $\pi/2$ with respect to the incident beam and then dispersed by a 1 m Jarrell−Ash Czerny−Turner double monochromator with an optical resolution of ~0.15 nm. The visible emissions from the sample exiting the monochromator were detected by a thermoelectrically cooled Hamamatsu R943−02 photomultiplier tube. A preamplifier, model SR440 Standard Research Systems, processed the photomultiplier signals and a gated photon-counter model SR400 Standard Research Systems data acquisition system was used as an interface between the computer and the spectroscopic hardware. The signal was recorded under computer control using the Standard Research Systems SR465 software data acquisition/analyzer system.

2.3. X-ray Powder Diffraction (XRPD) Analysis. XRPD patterns were measured using a Scintag XDS-2000 Diffractometer equipped with a Si(Li) Peltier-cooled solid state detector, Cu Kα source at a generator power of 45 kV and 40 mA, divergent beam (2 and 4 mm), and receiving beam slits (0.5 and 0.2 mm). Scan range was set from 20 to 80° 2θ with a step size of 0.02° and a count time of 2 s. The sample was measured using a quartz "zero background" disk.

2.4. Transmission Electron Microscopy (TEM) and Selected Area Electron Diffraction (SAED). TEM measurements of the colloidal dispersion of nanoparticles were performed with a Philips CM200 microscope operating at 200 kV equipped with a charge-coupled device (CCD) camera (Gaten). A minute amount of sample was dispersed in an appropriate amount of toluene to yield an approximate 0.1 wt % solution. A drop of the resulting solution was evaporated on a Formvar/carbon film supported on a 300 mesh copper grid (3 mm in diameter).

Results and Discussion

The thermal decomposition synthesis yields nanocrystals of $BaYF_5$:Tm^{3+} 0.5 mol%, Yb^{3+} 15 mol% capped with oleic acid that easily disperse in nonpolar solvents to form perfectly clear colloidal dispersions. The capping ligand is important, as it also allows for the controlled growth of the nanoparticle, controls the size of the nanoparticle, and prevents agglomeration. This is in contrast to uncapped nanopowders, where quenching due to surface defects is prevalent, resulting in significantly weaker luminescence compared to the bulk crystals. Although capping with oleic acid is not ideal for biological applications where dispersibility in water is of the essence, there exist a number of strategies to render hydrophobic nanoparticles hydrophilic, including ligand exchange and oxidation of the C=C bond of the oleic acid capping ligand.[12,23] The transmission electron microscopy (TEM) image of the $BaYF_5$:Tm^{3+}, Yb^{3+} nanocrystals is shown in Figure 1. The resulting nanocrystals were observed to be roughly rectangular in shape with an average size of about 15 nm across the long edge (and 5 nm wide).

(17) García Solé, J. ; Bausá, L. E.; Jaque, D. *An Introduction to the Optical Spectroscopy of Inorganic Solids*; John Wiley & Sons Ltd.: West Sussex, U.K., 2005.
(18) Johnson, L. F.; Geusic, J. E.; Guggenheim, H. J.; Kushida, T.; Singh, S.; Van Uitert, L. G. *Appl. Phys. Lett.* **1969**, *15*, 48–50.
(19) Guggenheim, H. J.; Johnson, L. F. *Appl. Phys. Lett.* **1969**, *15*, 51–52.
(20) Johnson, L. F.; Guggenheim, H. J.; Rich, T. C.; Ostermayer, F. W. *J. Appl. Phys.* **1972**, *43*, 1125–1137.
(21) Auzel, F. E. *Proc. IEEE* **1973**, *61*, 758–786.
(22) Zhang, Y. W.; Sun, X.; Si, R.; You, L. P.; Yan, C. H. *J. Am. Chem. Soc.* **2005**, *127*, 3260–3261.
(23) Zhang, T.; Ge, J.; Hu, Y.; Yin, Y. *Nano Lett.* **2007**, *7*, 3203–3207.

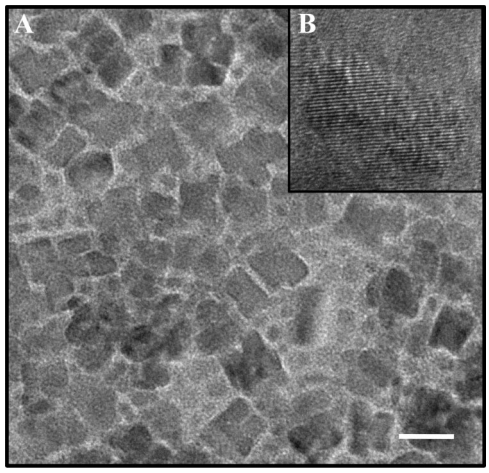

Figure 1. (A) Transmission electron microscopy (TEM) image of $BaYF_5$:Tm^{3+}, Yb^{3+} nanocrystals (scale bar = 15 nm). (B) High-resolution image of a single nanocrystal.

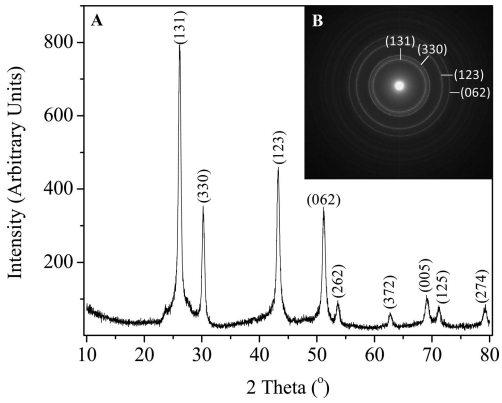

Figure 2. (A) X-ray powder diffraction (XRPD) pattern and (B) selected area electron diffraction (SAED) pattern of $BaYF_5$:Tm^{3+}, Yb^{3+} nanocrystals.

The inset in Figure 1 shows a high-resolution TEM image of a single particle where the lattice fringes are clearly observed alluding to the highly crystalline nature of the material. The distance between the lattice fringes (*d*-spacing) was measured to be 3.2 Å. The crystallinity was confirmed in the X-ray powder diffraction (XRPD) patterns shown in Figure 2A. The position of the peaks in the XRPD pattern of $BaYF_5$:Tm^{3+}, Yb^{3+} nanocrystals closely match those previously reported for $BaYF_5$, indicating that the nanoparticle lattice is in fact tetragonal.[24,25] The average crystallite size was calculated to be 16.8 nm using the Debye−Scherrer formula, which corresponds well with the TEM data. The selected area electron diffraction (SAED) pattern (Figure 2B) again demonstrated the highly crystalline nature of the material and confirmed the tetragonal crystalline structure of the $BaYF_5$:Tm^{3+}, Yb^{3+} nanocrystals.

$BaYF_5$:Tm^{3+}, Yb^{3+} nanocrystals yield a blue emission visible to the naked eye following excitation with 980 nm (at a power density of 90 W/cm^2) and is shown in Figure 3. The corresponding upconversion spectrum (Figure 3A) shows a weak emission in the indigo centered at about 452 nm and

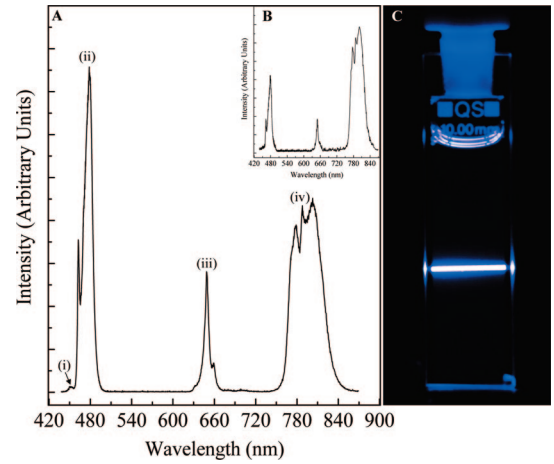

Figure 3. Upconversion emission spectrum of $BaYF_5$:Tm^{3+}, Yb^{3+} nanocrystals following excitation with 980 nm at (A) 90 and (B) 15 W/cm^2. (i) $^1D_2 \rightarrow {}^3F_4$, (ii) $^1G_4 \rightarrow {}^3H_6$, (iii) $^1G_4 \rightarrow {}^3F_4$, (iv) $^3H_4 \rightarrow {}^3H_6$. (C) Colloidal dispersion of $BaYF_5$:Tm^{3+} 0.5 mol %, Yb^{3+} 15 mol % nanocrystals in toluene (2 wt %) following excitation with 980 nm.

ascribed to the $^1D_2 \rightarrow {}^3F_4$ transition, whereas a very intense blue emission was observed centered at 475 and was assigned to the $^1G_4 \rightarrow {}^3H_6$ transition. Upconverted emission was also detected in the red and NIR regions of the spectrum and assigned to the $^1G_4 \rightarrow {}^3F_4$ (centered at 650 nm) and $^3H_4 \rightarrow {}^3H_6$ (centered at 800 nm) transitions, respectively.

The upconversion emission spectrum of $BaYF_5$:Tm^{3+}, Yb^{3+} nanocrystals differs markedly from other fluoride-based nanocrystals codoped with Tm^{3+} and Yb^{3+} reported in the literature. For example, $NaYF_4$:Tm^{3+}, Yb^{3+} nanocrystals have been studied in great detail.[14,26−28] Typically in this material, the NIR emission is significantly more intense than the blue and red upconversion emissions. This is strikingly different in the $BaYF_5$:Tm^{3+}, Yb^{3+} nanocrystals where the upconverted blue $^1G_4 \rightarrow {}^3H_6$ emission is the most intense peak, thus making this a potentially interesting material for applications such as display or luminescence devices where a strong blue emission is required.

Upconversion to the $^3H_4$ state resulting in the NIR $^3H_4 \rightarrow {}^3H_6$ transition (centered at 800 nm) occurs via a two-photon process (see Figures 4 and 5). That is, it occurs via two successive energy transfers from Yb^{3+} ions in the $^2F_{5/2}$ excited states. Specifically, an excited Yb^{3+} in the $^2F_{5/2}$ excited state transfers its energy nonresonantly to a Tm^{3+} ion in the $^3H_6$ ground-state thereby exciting it to the $^3H_5$ excited state (denoted as ① in Figure 5), after which it decays nonradiatively to the $^3F_4$ excited state. A second Yb^{3+} ion in close proximity then transfers its energy to the Tm^{3+} ion exciting it from the $^3F_4$ to the $^3F_2$ excited state (denoted as ② in Figure 5). The excited Tm^{3+} ion will subsequently decay nonradiatively to the $^3H_4$ state where it can emit an 800 nm photon radiatively following relaxation to the ground state. Alternatively, the Tm^{3+} ion can be excited nonresonantly via a third energy transfer from an excited Yb^{3+} ion to the $^1G_4$ state (denoted as ③

(24) Liu, F.; Wang, Y.; Chen, D.; Yu, Y.; Ma, E.; Zhou, L.; Huang, P. *Mater. Lett.* **2007**, *61*, 5022–5025.
(25) Yi, G. S.; Lee, W. B.; Chow, G. M. *J. Nanosci. Nanotechno.* **2007**, *7*, 2790–2794.
(26) Wang, F.; Chatterjee, D. K.; Li, Z.; Zhang, Y.; Fan, X.; Wang, M. *Nanotechnology* **2006**, *17*, 5786–5791.
(27) Yi, G. S.; Chow, G. M. *Adv. Funct. Mater.* **2006**, *16*, 2324–2329.
(28) Zhang, F.; Wan, Y.; Yu, T.; Zhang, F.; Shi, Y.; Xie, S.; Li, Y.; Xu, L.; Tu, B.; Zhao, D. *Angew. Chem., Int. Ed.* **2007**, *46*, 7976–7979.

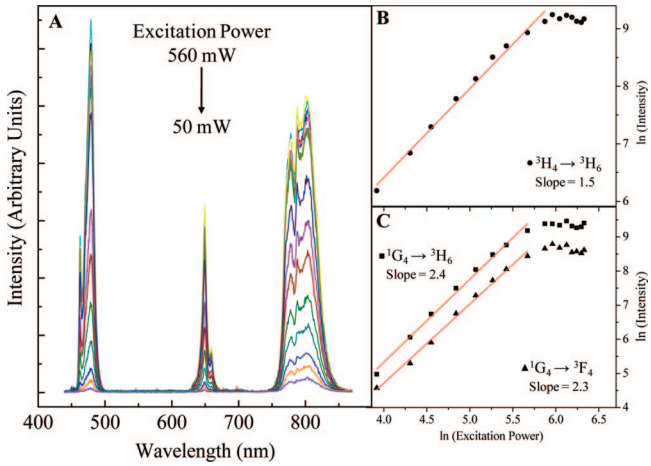

Figure 4. Power dependence study of the upconverted emissions in $BaYF_5$:Tm^{3+}, Yb^{3+} nanocrystals. (A) Upconversion spectra as a function of pump power from 560 mW (90 W/cm^2) to 50 mW (8 W/cm^2). (B, C) Graphs of ln (Intensity) versus ln (Excitation Power) for the upconverted emissions from the $^3H_4$ and $^1G_4$ excited states, respectively. At higher excitation densities, the emission intensity plateaus due to a saturation of the upconversion process.

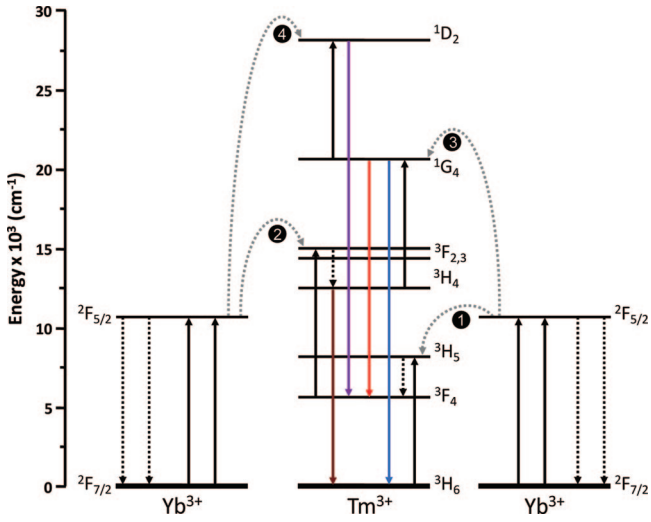

Figure 5. Mechanism of the upconversion process in Tm^{3+}, Yb^{3+} codoped nanocrystals following excitation with 980 nm. Black solid arrows represent the excitation process, whereas the straight and curly dotted arrows represent the nonradiative decay and energy transfer, respectively. The colored solid arrows represent the upconverted radiative emission. Note: Energy transfers 1, 3, and 4 are nonresonant and excess energy is dissipated by the lattice.

in Figure 5). It follows that because the $^3H_4$ excited-state is populated via a two-photon process whereas the $^1G_4$ state is populated via a three-photon mechanism, the NIR $^3H_4 \rightarrow {}^3H_6$ emission should be more intense than the blue $^1G_4 \rightarrow {}^3H_6$ transition because the probability of a two-photon mechanism is higher than that of a three-photon mechanism, as is observed in other Tm^{3+}-doped nanocrystals. Yet, this is not the case. Given the intensity of the upconverted blue $^1G_4$ emission, it is therefore very plausible that the excited-state absorption from the $^3H_4$ state is favored to the detriment of the $^3H_4$ radiative decay. However, there are other key factors involved and the reason for the intensity trends is still under investigation. Finally, a fourth Yb^{3+} transfer populates the $^1D_2$ excited state (denoted as ④ in Figure 5). However, because the intensity of this peak is extremely weak, it is safe to say that this final transfer occurs with little probability. This is very likely because the mismatch of energy between the $^2F_{7/2} \leftarrow {}^2F_{5/2}$ Yb^{3+} and $^1G_4 \rightarrow {}^1D_2$ Tm^{3+} transitions is greater than 3000 cm^{-1}.[20]

The power dependence study revealed an interesting fact (Figure 4). At low power densities, the upconversion spectrum of the $BaYF_5$:Tm^{3+}, Yb^{3+} nanocrystals following excitation with 980 nm (15 W/cm^2) resembled a more typical upconversion spectrum of Tm^{3+}, Yb^{3+} codoped nanocrystals where the NIR peak at 800 nm ($^3H_4 \rightarrow {}^3H_6$) is dominant (see Figure 3B). Furthermore, the $^1D_2 \rightarrow {}^3F_4$ emission is no longer observed. At high power densities, there are a sufficient number of excited Yb^{3+} ions that can sustain the Yb^{3+} energy transfer to populate the $^1G_4$ level. In fact at power densities above 355 mW (57 W/cm^2), the power dependence revealed a plateau, indicating that the upconversion process was in fact saturated (Figure 4 B, C). This saturation is attributed to the fact that the $^3F_4 \rightarrow {}^3F_2$ transition, following the second transfer of energy from an excited Yb^{3+} ion, is so efficient that it exceeds the spontaneous decay rate of the $^3F_4$ state.[20] Therefore, at low power densities, there are an insufficient number of excited Yb^{3+} ions and thus the two-photon upconversion process is favored, resulting in the relatively stronger NIR upconversion emission observed from the $^3H_4$ state.

It should also be noted that the observed slopes, which correspond to the number of photons required to populate the emitting state in the upconversion process (panels B and C in Figure 4), deviated from the expected values, according to the upconversion mechanism shown in Figure 5, where two photons are required to populate the $^3H_4$ state whereas three photons are required for the $^1G_4$ state. We obtained slopes of 2.4 and 2.3 for the upconverted emissions emanating from the $^1G_4$ state and a slope of 1.5 for the $^3H_4$ upconverted emissions. In an unsaturated upconversion process, $I \propto P^n$, where the upconverted luminescence intensity, I, is proportional to the nth power of the NIR excitation power, P. This relation typically holds only for low excitation powers; at high excitation densities, the upconversion processes will saturate. Upconversion is a nonlinear process and as a consequence of the conservation of energy, it cannot maintain its nonlinear behavior up to infinite excitation. Therefore, the power dependence does not follow the above straightforward relation at higher pump powers. Thus, we obtain slopes (n) from the graph of the natural logs of the intensity versus the excitation power, which deviated from the expected values in cases where the influence of upconversion is large (i.e., high pump densities).[29]

In summary, we have shown that tetragonal $BaYF_5$:Tm^{3+} 0.5 mol %, Yb^{3+} 15 mol % nanocrystals, synthesized via the thermal decomposition method, emit blue light following excitation with NIR radiation ($\lambda_{exc} = 980$ nm) via a process known as upconversion. The obtained nanocrystals were

(29) Pollnau, M.; Gamelin, D. R.; Lüthi, S. R.; Güdel, H. U. *Phys. Rev. B* **2000**, *61*, 3337–3346.

rectangular in shape and observed to be approximately 15 nm × 5 nm in size. The upconversion spectrum revealed that the peak attributed to the blue emission ($^1G_4 \rightarrow {}^3H_6$) was the most intense, more so than the upconverted NIR emission ($^3H_4 \rightarrow {}^3H_6$), contrary to what is normally observed in other Tm^{3+}/Yb^{3+} codoped nanomaterials. In contrast, at low power densities, the NIR emission is more intense than the blue indicating that there are not enough excited Yb^{3+} ions to sustain the population of the $^1G_4$ emitting state at these power densities. Furthermore, the upconversion process was shown to easily saturate, at excitation densities above 57 W/cm^2, leading to a deviation in the power dependence studies from the expected values ascertained from the upconversion mechanism.

Acknowledgment. The authors thank the Natural Sciences and Engineering Research Council (NSERC) of Canada and the Gouvernement du Québec, Ministère du Développement économique, de l'Innovation et de l'Exportation for funding.

CM900313S